Rapid Communications in Mass Spectrometry

WILEY

Rapid Communications in Mass Spectrometry

RESEARCH ARTICLE OPEN ACCESS

The Site of Protonation Affects the Dissociation of Protonated α- and β-Pinene Ions

Edgar White Buenger | Paul M. Mayer

Department of Chemistry and Biomolecular Sciences, University of Ottawa, Ottawa, Canada

Correspondence: Paul M. Mayer (pmmayer@uottawa.ca)

Received: 17 September 2024 | **Revised:** 10 December 2024 | **Accepted:** 16 December 2024

Funding: This work was supported by Natural Sciences and Engineering Research Council of Canada, RGPIN-2021-03175.

Keywords: collision-induced dissociation | computed minimum energy reaction pathways | protonation | tandem mass spectrometry | terpenes | unimolecular reactions | α-Pinene | β-Pinene

ABSTRACT

Rationale: In electrospray ionization and atmospheric pressure chemical ionization, the protonation site directly guides the ion's dissociation. But what if the site of protonation is ambiguous? In this study, we explored the unimolecular reactions of protonated α- and β-pinene ions with a combination of tandem mass spectrometry and theory. Each has multiple potential protonation sites that influence their chemistry.

Methods: Atmospheric pressure chemical ionization was employed to form the protonated pinene isomers. The unimolecular chemistry of these ions was explored with a Waters Ultima triple-quadrupole mass spectrometer using energy-resolved collision-induced dissociation with argon collision gas. Reaction mechanisms were calculated with CBS-QB3 single-point energy calculations on B3LYP/6-311+G(d,p) optimized structures.

Results: The two main dissociation reactions in each ion lead to the loss of neutral propene and isobutene. Both ions were found to dissociate over the same minimum energy reaction pathway, the only difference being the site of initial protonation. α-Pinene preferentially protonates at the bridging carbon, while β-pinene can only significantly protonate at the exocyclic double bond. This leads to a lower appearance energy for loss of isobutene, and thus relatively greater m/z 81 fragment ion abundance for β-pinene.

Conclusions: The distinct sites of initial protonation result in the subtle differences observed in the CID of α- and β-pinene. The work highlights that it is not necessarily the "lowest energy" ion that will be formed in the ion source, and any distribution of initial structures must be accounted for when examining CID mass spectra.

1 | Introduction

Monoterpenes are produced naturally through biosynthetic pathways available across a variety of plant species [1]. These compounds constitute the majority component of plant essential oils, an extract that captures and concentrates the plant's unique aroma and/or flavor. Aside from their natural production and function in plants, humans make extensive use of monoterpenes across a variety of industries [2–5]. Pinene is one of the most abundant monoterpenes and features a unique [6 + 4]-bicyclic structure that has two prominent isomers: the α isomer bearing an endocyclic double bond, and the β isomer bearing an exocyclic one (Figure 1). Anthropogenically, the pinene isomers offer an excellent starting point for the organic synthesis of more complex natural products and pharmaceuticals [6]. In addition, there has been evidence showing that the pinene isomers themselves have broad-ranging therapeutic effects [7]. A significant consequence resulting from both natural and human sources of monoterpene production is the emission of gaseous terpenes into the atmosphere, estimated

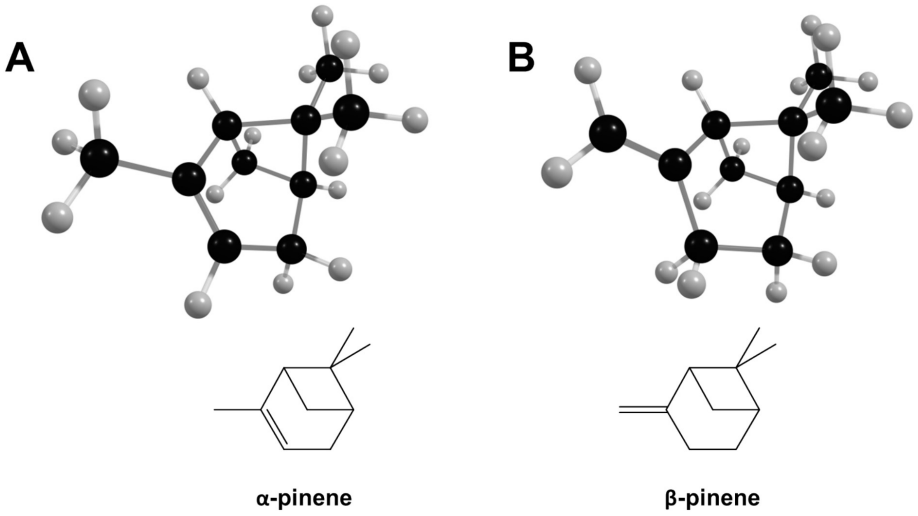

FIGURE 1 | Optimized minimum energy structures obtained for (A) neutral α-pinene and (B) neutral β-pinene calculated at the B3LYP/6-311+G(d,p) level of theory. 2-dimensional stick diagrams have been included to assist with visual clarity of the double bond position.

to be in the range of 26–156 Tg per year, of which the pinene isomers contribute a large portion [8]. Atmospheric reactions of pinene include a wide variety of oxidation reactions that contribute towards secondary organic aerosol formation [9–13].

There remain relatively unexplored avenues of pinene chemistry, for instance, protonation of gaseous pinenes and reactions that result from this protonation. It has been demonstrated that α-pinene can react on the surface of acidic aerosols, leading to the occurrence of polymerization reactions [14]. Another study demonstrated that the abundance of pinene isomers can be observed to decrease on the surface of sulfuric acid solutions, coinciding with the appearance of a smaller mass product, suggesting that the acidic solution may protonate the pinenes and subsequently lead towards fragmentation [15]. It has also been reported that gaseous pinene may protonate on the surface of acidic water and ethanol clusters, leading to the stabilization of a protonated pinene-water cluster complex, which may undergo further reactions [16, 17].

It has previously been shown that the site of protonation can significantly impact the fragmentation of organic molecules in mass spectrometry, where there are multiple sites within the molecule that can accept a proton [18, 19]. A few research groups have attempted to perform positively charged mass spectrometry experiments involving protonated terpenes. One paper showed that there was minimal differences between the pinene isomers with regard to product ion abundances, with a dominant *m/z* 137 precursor ion and *m/z* 81 product ion, and included the presence of some minor products at *m/z* 138, 95, and 82 [20]. However, the authors did not explore the mechanisms of formation of these product ions. Another group attempted to use proton transfer mass spectrometry to differentiate isomeric monoterpenes, including α-, and β-pinene, noting marginal differences owing to the position of the double bond [21]. Research that has come out of our group has demonstrated that the site of protonation can significantly impact the fragmentation of protonated terpenes [22–24]. This paper will aim to further understand the chemistry that occurs following the protonation of the two most abundant isomers of pinene, through a combination of tandem mass spectrometry and density functional theory calculations.

2 | Experimental Procedures

2.1 | Sample Preparation

Both compounds were used as purchased, without further purification, were prepared as individual solutions in methanol, and diluted to 100 μg/mL prior to injection into the mass spectrometer.

2.2 | Tandem Mass Spectrometry

Solutions were introduced into the Waters Quattro Ultima triple quadrupole mass spectrometer (Waters, Manchester, UK) using a syringe pump operating at a flow rate of 50 μL/min. An atmospheric pressure chemical ionization (APCI) source was used to generate protonated α-pinene and protonated β-pinene, with the probe set to a temperature of 200 °C, the source operating at 100 °C and the corona discharge needle set to 10 μA, operating in the positive ionization mode. Desolvation gas (N_2) was set to a flow rate of 36 L/h. The collision-induced dissociation (CID) experiment was performed by reducing the main precursor ion beam signal intensity by 50 % through the addition of argon gas in the collision cell. The CID experiments were performed using 0–20 eV of collision energy (laboratory frame, E_{Lab}), at intervals of 1 eV.

2.3 | Breakdown Diagrams

The collection of CID data was compiled into breakdown diagrams, where the relative abundance of the ions observed in the CID mass spectra are plotted as a function of increasing collision energy. To compare the breakdown behaviour of different ions more accurately, the collision energy applied by the

instrument (E_{Lab}) is first converted to the center-of-mass frame of reference (E_{CoM}). This conversion accounts for differences in the efficiency of energy transfer during the collisional activation, according to Equation 1 below:

$$E_{CoM} = E_{Lab}\left(\frac{m_{Ar}}{m_{Ar} + m_I}\right) \quad (1)$$

where m_{Ar} is the mass of argon and m_I is the mass of the ion undergoing CID.

2.4 | Computational Methods

All calculations (geometry optimizations and vibrational frequency calculations and intrinsic reaction coordinate) were performed with the GAUSSIAN 16 suite of programs at the B3LYP/6-311+G(d,p) level of theory [25–27]. The B3LYP output files were used for single-point energy calculations using the CBS-QB3 composite method, to provide more accurate energy values [28, 29]. Transition state structures featuring a single negative vibrational mode were verified using intrinsic reaction coordinate calculations. The optimized geometries and internal energies obtained through these sets of calculations were used to produce minimum energy reaction pathways (MERP). In these models, the pathway from reactants to products was mapped through the individual transformations involved (transition states, intermediates, and ion-molecule complexes). All relative energies are reported at 0 K and all processes are described in terms of energy (eV). The structure marked as zero energy is considered the baseline to which others are compared.

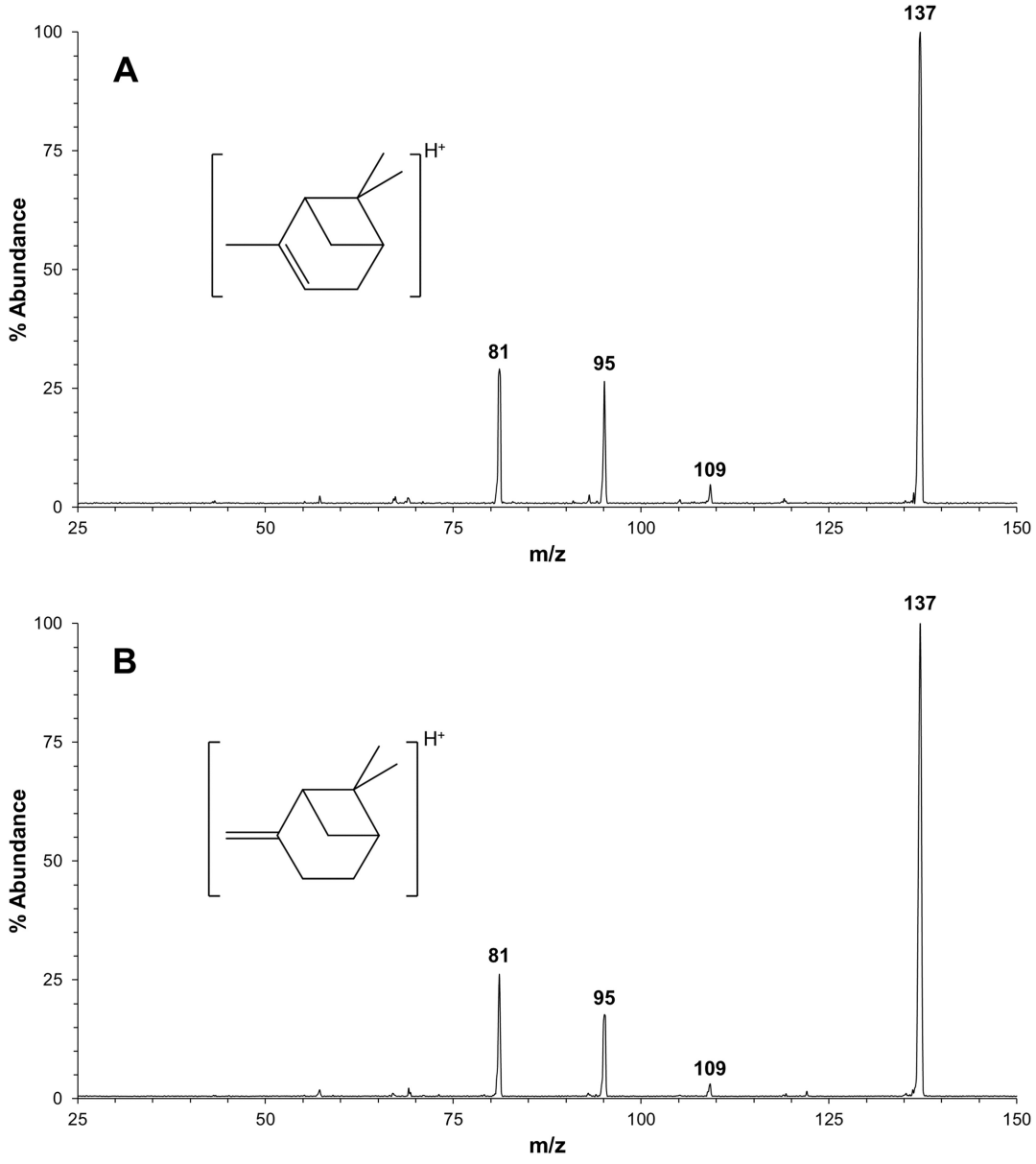

FIGURE 2 | Representative CID-MS/MS spectra obtained from (A) protonated α-pinene and (B) protonated β-pinene, where the collision energy was set to 10 eV in both cases.

3 | Results and Discussion

3.1 | Tandem Mass Spectrometry and Breakdown Diagrams

Representative mass spectra that were obtained during the collection of CID-MS/MS experiments performed on protonated α-, and β-pinene are presented in Figure 2, labeled with the precursor ion (*m/z* 137), and the most prominent product ions at *m/z* 81, 95, and 109. There is little difference between the fragmentation of the two protonated pinene isomers. There appears to be a slightly greater abundance of *m/z* 95 in the fragmentation of protonated α-pinene when compared to protonated β-pinene. Numerous minor product ions can be seen in both spectra, although there appears to be a greater variety of minor fragments observed in the case of α-pinene, and the abundance of these ions does not exceed 1%. The CID-MS/MS mass spectra were compiled into breakdown diagrams, Figure 3. At low collision energy (under 1 eV), *m/z* 81 is the only ion observed for both protonated pinenes. The *m/z* 95 product ion begins to appear at approximately 1 eV and is slightly more abundant in protonated α-pinene as the collision energy increases. The most abundant of the minor product

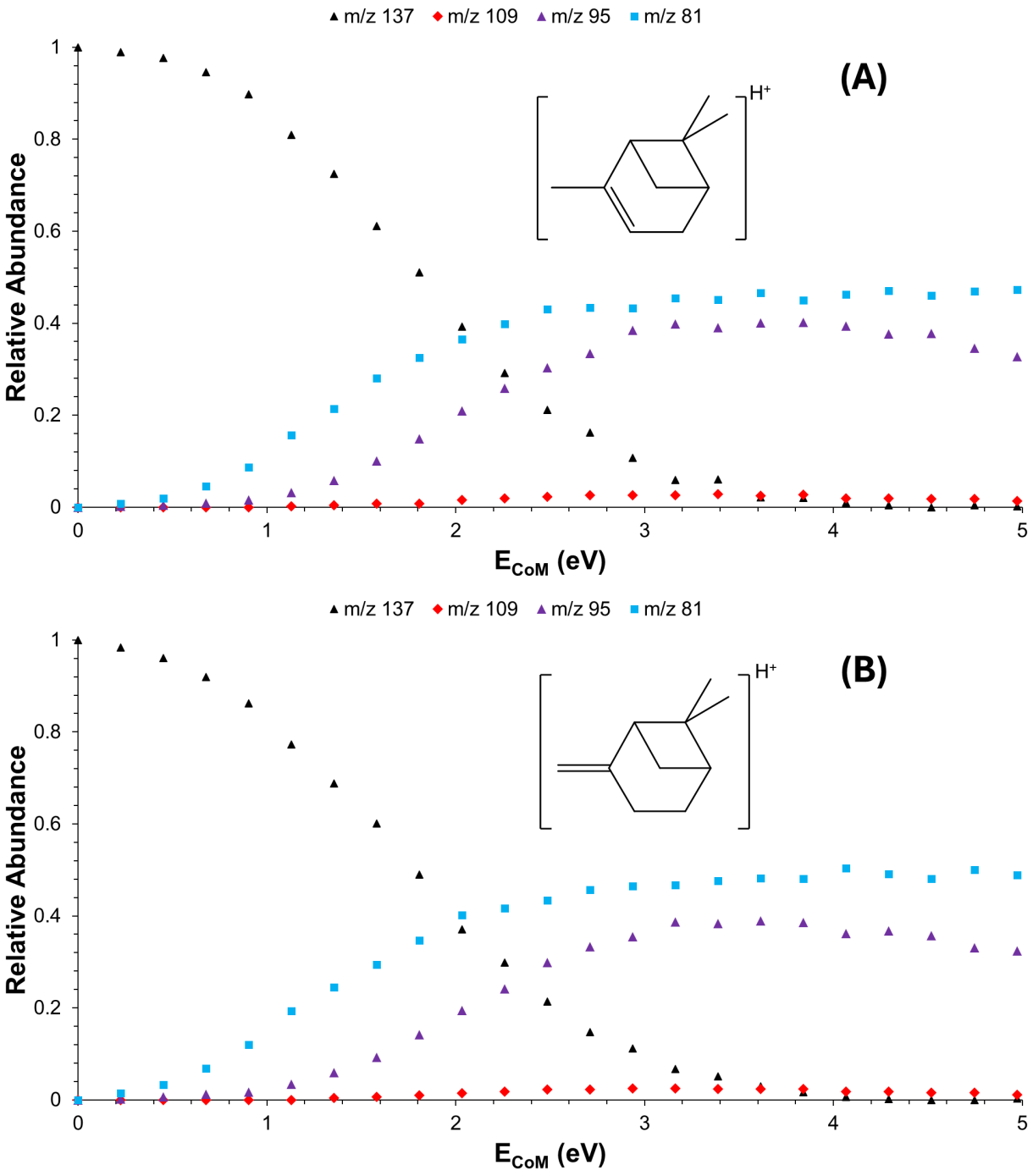

FIGURE 3 | CID breakdown curves obtained from protonated α-pinene (A), and protonated β-pinene (B). The data was consistent across two separate measurement days.

ions, *m/z* 109, was included in the breakdown diagram, and can be observed between 2–5 eV, however, its abundance does not exceed 3% at any point throughout the experiment.

3.2 | Minimum Energy Reaction Pathways

The calculated reaction pathways for *m/z* 81 and 95 are presented in Figure 4. Both compounds are represented within the figure, although they differ by which species along the path they populate in the ion source. In the case of *m/z* 95, the reaction begins through protonation of neutral α-pinene at the CH_2 carbon of the four-membered ring, leading to structure **1a**, set as the relative zero energy structure for the reaction pathways. The reaction proceeds through **TS1a-1b** where one of the protons from the CH_3 group formed in the previous step undergoes a 1,4-H shift, leading to the structure **1b**, featuring a four-membered ring. From **1b**, the reaction proceeds through a sequence of low energy barrier bond stretching transition states that ultimately lead to structure **1e**, where the four-membered ring has been broken to yield an exocyclic propyl moiety and sits at 0.30 eV. From the intermediate **1e,** the reaction continues towards an ion-molecule complex through the transition state **TS1e-1f** where the exocyclic propyl undergoes a 1,2-H shift, landing at **1f**. The reaction completes through dissociation of the two species that produce the neutral loss of C_3H_6 and the observed ion at m/z 95.

The pathway leading to *m/z* 81 can also be observed in Figure 4, labeled in purple. This reaction pathway begins from the intermediate **1b**, which passes through a transition state **TS1b-1c** at 1.16 eV, where one of the CH_2 carbons that is part of the four-membered ring can undergo a 1,2-H shift, leading to the ion-molecule complex **1c**. The reaction completes through the loss of neutral C_4H_8, leaving the observed ion at *m/z* 81, a protonated methylcyclopentadiene.

3.3 | Relating Theoretical Reaction Pathways to the Experimental Observations

The CID-MS/MS experiment of the protonated pinenes can first be related to the theoretically calculated minimum energy reaction pathways by the initial site of protonation of each of the neutral pinene species. In each of the two neutral pinene isomers, five carbons may reasonably accept a proton

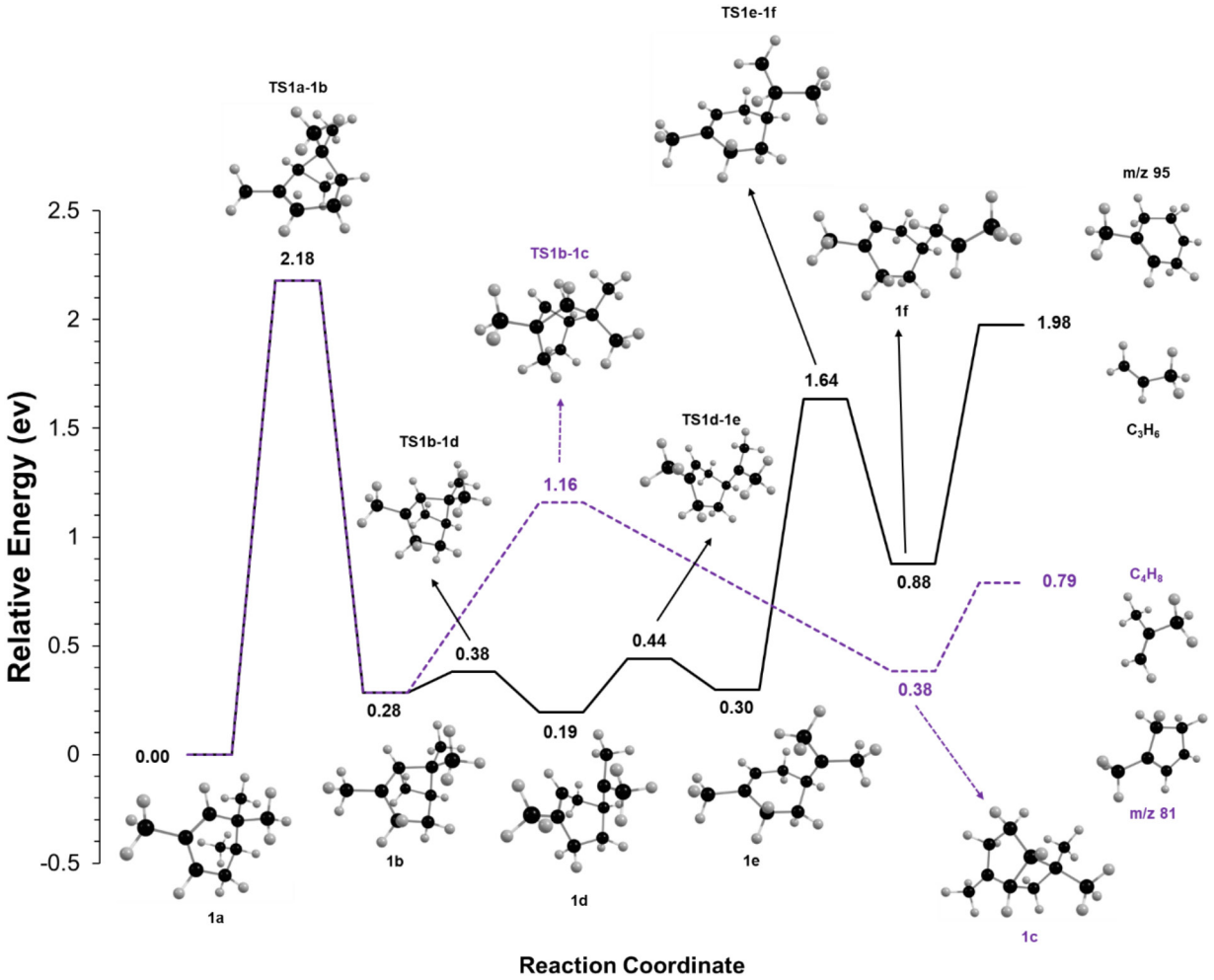

FIGURE 4 | CBS-QB3(sp)//B3LYP/6-311+G(d,p) calculated minimum energy reaction pathways that include the major product ions observed in the breakdown of both protonated α-pinene and protonated β-pinene. The pathways have been differentiated by color, where the black pathway leads towards m/z 95 and C_3H_6 loss and the purple pathway leads towards m/z 81 and C_4H_8 loss.

in the ion source, including the double-bond bearing carbons and the carbons of the four-membered ring system (Figure 1). For α-pinene, four structures may be produced via protonation of these five carbons, two of which are represented in the minimum energy reaction pathways as **1a**, and **1b** (Figure 4 & Figure S1). Thus, the initial protonation of α-pinene would be expected to nearly exclusively populate **1a**, with a fractional proportion of **1b** being produced. In comparison, the β-pinene isomer has four protonated structures that may be formed from protonation at the five positions, however only one of these structures is found on the minimum energy reaction pathway (**1b**). The remaining structures are relatively higher in energy, only βS3 has the possibility of being marginally populated following protonation and has been determined not to contribute towards the observed reaction pathways (Figure S2). Thus, the chemistry of protonation of β-pinene would exclusively start from populated structure **1b** on the reaction surface. This difference in the starting point along the reaction coordinate for each of the isomers explains the slightly different relative abundances of *m/z* 81 and 95 in the protonated β-pinene breakdown (Figure 3). **1b** can immediately access the key transition state **TS1b-1c** that leads towards the *m/z* 81 ion, compared with **1a,** which must first overcome the energetically higher **TS1a-1b** to access the two fragmentation channels (Figure 4). Dissociating protonated α-pinene ions thus have a higher average internal energy, leading to slightly more *m/z* 95 forming.

4 | Conclusions

The unimolecular chemistry of the protonated bicyclic monoterpenes α-pinene and β-pinene were investigated using a combined experimental and theoretical approach, encompassing CID-MS/MS and density functional theory calculations. The CID breakdown experiments led to nearly identical fragmentation for both isomers, with subtle differences. Two prominent product ion pathways were observed at m/z 95 and 81, corresponding to the neutral losses of propene and isobutylene, respectively. Calculations revealed that the observed products for each protonated isomer were dependent upon the site of protonation. The α-isomer initially populates a slightly more stable structure, which requires an initial transformation before reaching the reactive intermediate **1b**, whereas the β-isomer initially populates **1b** directly. This extra step may explain the two isomers' different relative fragment ion abundances.

Author Contributions

Edgar White Buenger: investigation, writing – original draft, writing – review and editing, methodology, formal analysis, data curation, validation. **Paul M. Mayer:** conceptualization, funding acquisition, writing – review and editing, methodology, software, project administration, supervision, resources.

Acknowledgments

PMM thanks the Natural Sciences and Engineering Research Council of Canada for continuing financial support, and the Digital Research Alliance of Canada for computational resources.

Data Availability Statement

The data that support the findings of this study are available from the corresponding author upon reasonable request.

Supporting Information Available

A PDF file with the structures formed by protonating the various carbons in α-pinene (Figure S1) and β-pinene (Figure S2).

References

1. A. Cheng, Y. Lou, Y. Mao, S. Lu, L. Wang, and X. Chen, "Plant Terpenoids: Biosynthesis and Ecological Functions," *Journal of Integrative Plant Biology* 49, no. 2 (2007): 179–186, https://doi.org/10.1111/j.1744-7909.2007.00395.x.

2. J.-D. Woodroffe, D. V. Lupton, M. D. Garrison, E. M. Nagel, M. J. Siirila, and B. G. Harvey, "Synthesis and Fuel Properties of High-Energy Density Cyclopropanated Monoterpenes," *Fuel Processing Technology* 222 (2021): 106952, https://doi.org/10.1016/j.fuproc.2021.106952.

3. J. F. R. De Alvarenga, B. Genaro, B. L. Costa, E. Purgatto, C. Manach, and J. Fiamoncini, "Monoterpenes: Current Knowledge on Food Source, Metabolism, and Health Effects," *Critical Reviews in Food Science and Nutrition* 63, no. 10 (2023): 1352–1389, https://doi.org/10.1080/10408398.2021.1963945.

4. A. Sarkic and I. Stappen, "Essential Oils and Their Single Compounds in Cosmetics—A Critical Review," *Cosmetics* 5, no. 1 (2018): 11, https://doi.org/10.3390/cosmetics5010011.

5. A. Koziol, A. Stryjewska, T. Librowski, et al., "An Overview of the Pharmacological Properties and Potential Applications of Natural Monoterpenes," *Mini-Reviews in Medicinal Chemistry* 14, no. 14 (2015): 1156–1168, https://doi.org/10.2174/1389557514666141127145820.

6. R. J. Nyamwihura and I. V. Ogungbe, "The Pinene Scaffold: Its Occurrence, Chemistry, Synthetic Utility, and Pharmacological Importance," *RSC Advances* 12, no. 18 (2022): 11346–11375, https://doi.org/10.1039/D2RA00423B.

7. B. Salehi, S. Upadhyay, I. Erdogan Orhan, et al., "Therapeutic Potential of α- and β-Pinene: A Miracle Gift of Nature," *Biomolecules* 9, no. 11 (2019): 738, https://doi.org/10.3390/biom9110738.

8. J. C. Acosta Navarro, S. Smolander, H. Struthers, et al., "Global Emissions of Terpenoid VOCs From Terrestrial Vegetation in the Last Millennium," *Journal of Geophysical Research-Atmospheres* 119, no. 11 (2014): 6867–6885, https://doi.org/10.1002/2013JD021238.

9. S. Iyer, M. P. Rissanen, R. Valiev, et al., "Molecular Mechanism for Rapid Autoxidation in α-Pinene Ozonolysis," *Nature Communications* 12, no. 1 (2021): 878, https://doi.org/10.1038/s41467-021-21172-w.

10. J. Peeters, L. Vereecken, and G. Fantechi, "The Detailed Mechanism of the OH-Initiated Atmospheric Oxidation of α-Pinene: A Theoretical Study," *Physical Chemistry Chemical Physics* 3, no. 24 (2001): 5489–5504, https://doi.org/10.1039/b106555f.

11. S. X. Ma, J. D. Rindelaub, K. M. McAvey, et al., "α-Pinene Nitrates: Synthesis, Yields and Atmospheric Chemistry," *Atmospheric Chemistry and Physics* 11, no. 13 (2011): 6337–6347, https://doi.org/10.5194/acp-11-6337-2011.

12. T. Nah, J. Sanchez, C. M. Boyd, and N. L. Ng, "Photochemical Aging of α-Pinene and β-Pinene Secondary Organic Aerosol Formed From Nitrate Radical Oxidation," *Environmental Science & Technology* 50, no. 1 (2016): 222–231, https://doi.org/10.1021/acs.est.5b04594.

13. D. Zhang and R. Zhang, "Ozonolysis of α-Pinene and β-Pinene: Kinetics and Mechanism," *Journal of Chemical Physics* 122, no. 11 (2005): 114308, https://doi.org/10.1063/1.1862616.

14. J. Liggio, S. Li, J. R. Brook, and C. Mihele, "Direct Polymerization of Isoprene and A-Pinene on Acidic Aerosols," *Geophysical Research*

Letters 34, no. 5 (2007): 2006GL028468, https://doi.org/10.1029/2006GL028468.

15. Z. Liu, M. Ge, S. Yin, and W. Wang, "Uptake and Reaction Kinetics of α-Pinene and β-Pinene With Sulfuric Acid Solutions," *Chemical Physics Letters* 491, no. 4–6 (2010): 146–150, https://doi.org/10.1016/j.cplett.2010.04.004.

16. F. Dhooghe, C. Amelynck, J. Rimetz-Planchon, N. Schoon, and F. Vanhaecke, "FA-SIFT Study of Reactions of Protonated Water and Ethanol Clusters With α-Pinene and Linalool in View of Their Selective Detection by CIMS," *International Journal of Mass Spectrometry* 290, no. 2–3 (2010): 106–112, https://doi.org/10.1016/j.ijms.2009.12.010.

17. J. Poštulka, P. Slavíček, A. Domaracka, A. Pysanenko, M. Fárník, and J. Kočišek, "Proton Transfer From Pinene Stabilizes Water Clusters," *Physical Chemistry Chemical Physics* 21, no. 26 (2019): 13925–13933, https://doi.org/10.1039/C8CP05959D.

18. Y.-P. Tu, "Dissociative Protonation Sites: Reactive Centers in Protonated Molecules Leading to Fragmentation in Mass Spectrometry," *Journal of Organic Chemistry* 71, no. 15 (2006): 5482–5488, https://doi.org/10.1021/jo060439v.

19. N. Hu, Y.-P. Tu, Y. Liu, K. Jiang, and Y. Pan, "Dissociative Protonation and Proton Transfers: Fragmentation of α, β-Unsaturated Aromatic Ketones in Mass Spectrometry," *Journal of Organic Chemistry* 73, no. 9 (2008): 3369–3376, https://doi.org/10.1021/jo702464b.

20. A. Tani, S. Hayward, and C. N. Hewitt, "Measurement of Monoterpenes and Related Compounds by Proton Transfer Reaction-Mass Spectrometry (PTR-MS)," *International Journal of Mass Spectrometry* 223–224 (2003): 561–578, https://doi.org/10.1016/S1387-3806(02)00880-1.

21. P. K. Misztal, M. R. Heal, E. Nemitz, and J. N. Cape, "Development of PTR-MS Selectivity for Structural Isomers: Monoterpenes as a Case Study," *International Journal of Mass Spectrometry* 310 (2012): 10–19, https://doi.org/10.1016/j.ijms.2011.11.001.

22. E. White Buenger and P. M. Mayer, "Unraveling the Unimolecular Ion Chemistry of Protonated Isoprene and Prenol," *Journal of the American Society for Mass Spectrometry* 35, no. 1 (2024): 31–39, https://doi.org/10.1021/jasms.3c00297.

23. E. White Buenger, K. Mansour, and P. M. Mayer, "Exploring the Unimolecular Chemistry of Protonated Limonene and α-Terpineol," *International Journal of Mass Spectrometry* 498 (2024): 117204, https://doi.org/10.1016/j.ijms.2024.117204.

24. E. W. Buenger and P. M. Mayer, "Where You Protonate Matters: Deciphering the Unimolecular Chemistry of Protonated Myrcene and Linalool," *Journal of Mass Spectrometry* 59, no. 10 (2024): e5096, https://doi.org/10.1002/jms.5096.

25. M. J. Frisch, G. W. Trucks, H. B. Schlegel, et al., Gaussian 16 Rev. C.01, (2016).

26. A. D. Becke, "Density-functional Thermochemistry. III. The Role of Exact Exchange," *Journal of Chemical Physics* 98, no. 7 (1993): 5648–5652, https://doi.org/10.1063/1.464913.

27. C. Lee, W. Yang, and R. G. Parr, "Development of the Colle-Salvetti Correlation-Energy Formula Into a Functional of the Electron Density," *Physical Review B* 37, no. 2 (1988): 785–789, https://doi.org/10.1103/PhysRevB.37.785.

28. J. W. Ochterski, G. A. Petersson, and J. A. Montgomery, "A Complete Basis Set Model Chemistry. V. Extensions to Six or More Heavy Atoms," *Journal of Chemical Physics* 104, no. 7 (1996): 2598–2619, https://doi.org/10.1063/1.470985.

29. J. A. Montgomery, M. J. Frisch, J. W. Ochterski, and G. A. Petersson, "A Complete Basis set Model Chemistry. VI. Use of Density Functional Geometries and Frequencies," *Journal of Chemical Physics* 110, no. 6 (1999): 2822–2827, https://doi.org/10.1063/1.477924.

Supporting Information

Additional supporting information can be found online in the Supporting Information section.